FRET-sensing of multivalent protein binding at the interface of targeted biomimetic microparticles functionalized with tunable fluorescent lipids

Sophie Michelis,[1] Chiara Pompili,[2] Florence Niedergang,[2] Jacques Fattaccioli,[3,4] Blaise Dumat,[1*] Jean-Maurice Mallet[1*]

[1] Laboratoire des biomolécules, LBM, Département de chimie, École normale supérieure, PSL University, Sorbonne Université, CNRS, 75005 Paris, France

[2] Université Paris Cité, Institut Cochin, INSERM, CNRS, Paris, 75014, France

[3] PASTEUR, Département de Chimie, École Normale Supérieure, PSL Université, Sorbonne Université, CNRS, 75005 Paris, France

[4] Institut Pierre-Gilles de Gennes pour la Microfluidique, 75005 Paris, France

ABSTRACT

Cell adhesion is a fundamental phenomenon for cell communication and regulation. Adhesion sites are triggered by the binding of single ligand-receptor pairs that will initiate the formation of clusters of receptors. To study cell adhesion in live cells with microscopy techniques, there is a need of fluorescent particles targeted towards membrane receptors with a signal sensitive to the binding and movement of receptors and ligands at the interface. We propose new biomimetic fluorescent lipid microparticles for membrane receptor targeting and sensing. The particles are functionalized with tailor-made fluorescent lipids targeted towards lectins or biotin membrane receptor and can be specifically recognized and internalized by cells as evidenced by their phagocytosis in primary murine bone-marrow derived macrophages. By using a FRET pair of fluorescent mannolipids, it was possible to detect the presence of concanavalin A in solution by energy transfer showing that the particles can sense receptor binding at the interface and the associated movement of the ligands at the site of adhesion. Our results demonstrate that this biosensing platform can be specifically internalized by phagocytes, effectively mimicking a bacteria, and reveal short-range interactions of surface receptors via FRET.

1. INTRODUCTION

Cell adhesion is a fundamental phenomenon involved in stimulating signals that regulate cell differentiation, cell cycle, cell migration, and cell survival.[1] It promotes cell-cell adhesion, allows the detection of pathogens and the initiation of phagocytosis via the signaling by membrane receptors and antibody recruitment.[2,3,4] The specific recognition of molecular

patterns such as lipids, proteins or sugars at the surface of cells or bacteria by multivalent membrane receptors or clustering of these receptors leading to adhesion is a key in this biological process. Among those patterns, sugars are widely spread in biological organisms and can be bound by glycan-binding proteins, called lectins, and antibodies. They participate in the signaling of cells, the regulation of cell adhesion, in phagocytosis and in the developmental pathways.[5]

Micrometric carbohydrate coated materials can thus be used as simplified biomimetic materials to trigger adhesion and study associated biological processes (*e.g.* recognition, internalization). The affinity of the cell receptors for recognition patterns present at the surface of particles is a crucial consideration in designing targeted particles. The rigidity of the surface, the density of the ligands and the size appear to play a key role in recognition and internalization by cells and particularly by macrophages.[6,7,8] . Over the past few years, different solid and liquid particles have been developed to study the recognition or the immune response depending on the shape and size of the particle. There has been a major focus on solid glycosylated materials to promote the delivery of drugs and to target macrophages with platforms such as glycosylated quantum dots, silica nanomaterials, gold nanoparticles and amphiphilic polymer particles.[9,10] Liquid particles for cell targeting include mannosylated liposomes[11] or oil-in-water (O/W) droplets.[12] They have several advantages compared to solid glycomaterials. As interfacial particles, they can be coated with targeting moieties and these ligands are mobile on the liquid interface, allowing their clustering at the cell contact and thus increasing the affinity and recognition. Among liquid particles, liposomes are often chosen because their lipid bilayer resembles that of a cell. However, O/W droplets present several advantages: made from vegetable oil they can be formulated with biocompatible surfactants such as sugar-based surfactants polymers and thanks to their ambivalence, being stiff but also deformable, they favor recognition and cell adhesion without the need for a long spacer usually found in liposomes formulations.[13,14] For all these reasons, O/W droplets have been chosen here to develop a versatile platform using glycolipids and biotin lipids as surfactants.

To study cell adhesion in live cells with microscopy techniques, there is a need of fluorescent biomimetic particles with a signal sensitive to the binding and movement of receptors and ligands at the interface. Among fluorescence sensing modalities, FRET (Förster Resonance Energy Transfer) is widely used to evidence biological phenomena. Since it uses the nanometer scale energy transfer between two fluorophores, it gives valuable information on

short-range interactions well below the diffraction limit of fluorescence microscopy and would be particularly useful to evidence ligand clustering and/or receptor binding during adhesion processes. Yet despite, numerous instances of FRET applications inside of nanoparticules to demonstrate drug delivery or formation of nanoparticles,[15,16] inside liposomes to study the organization of the membrane,[17]or inside nano or micro emulsions,[18,19,20] energy transfer has, to the best of our knowledge, never been used at the surface of particles to monitor interfacial interactions and ligands movements upon interaction with a receptor.

Based on our experience in surface functionalization and glycolipid synthesis,[14,21] we designed in this work a biomimetic sensing platform composed of tailor-made lipids inserted at the interface of micrometric O/W droplets to target membrane receptors and study cell adhesion (Figure 1). The glycosylated particles are specifically recognized and internalized by phagocytic cells and the recognition and the clustering of ligands at the interface upon multivalent lectin binding can be detected by FRET between a matching pair of fluorophores incorporated in the tail of the lipids.

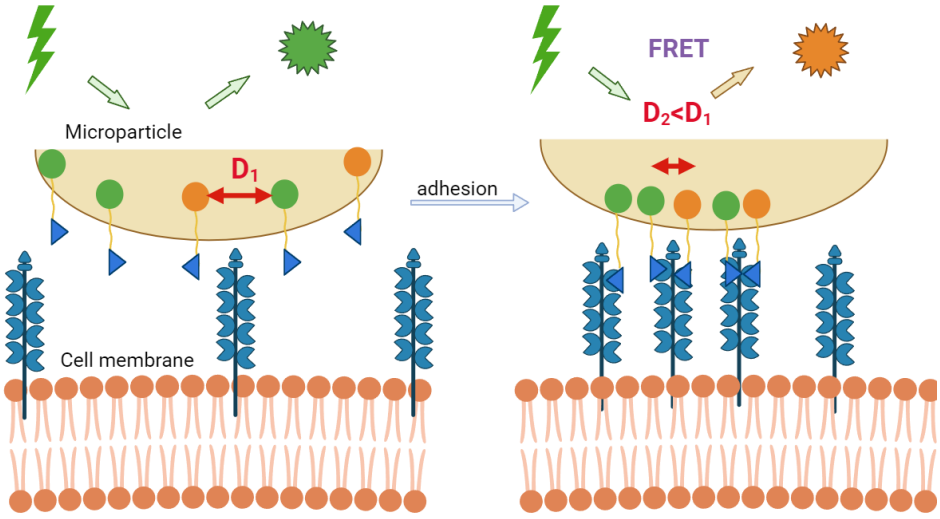

Figure 1: Schematic representation of the droplets and of the use of FRET to visualize receptor engagement for adhesion.

2. RESULTS AND DISCUSSION

Design and spectroscopic characterization of the fluorescent lipids. To functionalize the surface of micrometric lipid droplets we have designed amphiphilic linear lipids. The linear glycolipids are composed of 3 parts, as presented in Scheme 1: (i) a hydrophobic fluorophore, (ii) a lipid chain and (iii) a polar targeting head. This linear design is inspired by the structure

of natural glycolipids.[22] It is expected to enable the formation of an oriented layer at the water/droplet interface. The fluorophores stay inside the droplet and the sugar or biotin is exposed at the interface in water to enable selective recognition of the receptors. The fluorophores are built from the BODIPY scaffold, chosen for its lipophilicity, excellent photophysical properties (high brightness and photostability) and tunable absorption and emission wavelengths.[23,24,25] We synthesized a green-emitting BODIPY (G-mannolipid) by incorporating methyl groups at positions 1, 7, 3, and 5. Through a mono-coupling Knoevenagel reaction at position 3 with anisaldehyde, we obtained an orange-emitting BODIPY (O-mannolipid). For the lipid chain, a 12-amino lauric acid was chosen. Combined with the BODIPY, it is expected to have a similar lipophilia as C18 chains of natural lipids as BODIPY are highly hydrophobic fluorophores. The third part of the molecule aims at targeting glycan-binding proteins. To reach this goal a propargylamine was coupled to the carboxylic acid and a mannose was introduced via a CuAAC click reaction yielding the G-mannolipid and O-mannolipid compounds. Mannose-binding proteins recognize polysaccharide motifs and display very low affinities for monosaccharide. However, the use of liquid particles enables the mobility and the clustering of several monovalent ligands at the interface and we have previously shown that a simple mannose is sufficient to have an affine and selective recognition by these receptors.[14] A negative control lipid bearing a lactolipid that is not recognized by mannose receptors (G-lactolipid) was synthesized using the same procedure.

It has been reported in the literature that BODIPYs due to their structure, can form aggregates at high concentration which modify their fluorescence properties [26,27,28] and could be detrimental given the high local concentration that may be encountered on the surface of the droplets as in nanoparticles.[29] To study how the whole lipid structure impacts the organization at the interface and find the best structure for each BODIPY lipid involved in the FRET tool we have synthesized two additional green and orange mannolipid bearing negative charges close to the polar head (G-mannolipid (-) and O-mannolipid(-)). Due to the electrostatic repulsion, this charge is expected to modify the organization of BODIPYs on the surface. In addition, this charge will also modulate the amphiphilicity of the glycolipids and may thus affect the droplets formulation and receptor recognition. After obtaining the lauric acid BODIPY, a glutamate function was added to introduce a charge in the molecule. The charged G-mannolipid (-) and O-mannolipid (-) were obtained after deprotection with TFA in a modest yield due to the instability of BODIPY in acid conditions.

Finally, and to target other adhesion receptors, an amino PEGylated biotin was coupled to the lauric acid leading to G-biotinlipid. The PEG moiety was introduced to enhance the hydrophilic properties of the biotin

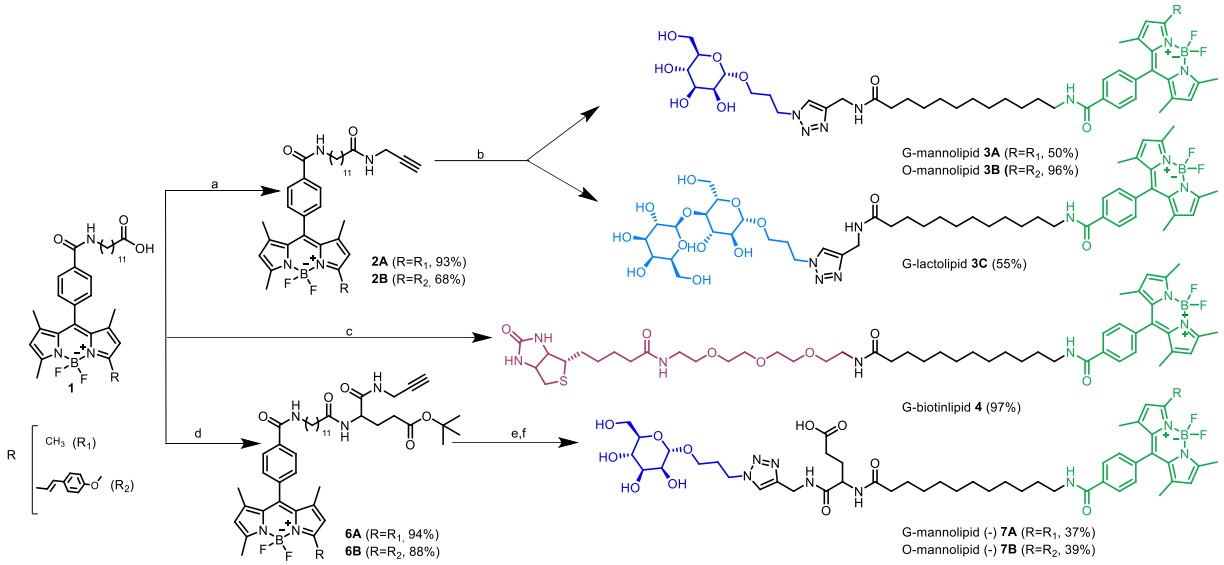

(a) propargylamine, DIEA, HATU, DMF; (b) Cu(I), azido-mannose or azido-lactose, DMF/H2O; (c) NH2-PEG$_3$-biotin, DIEA, HATU, DMF; (d) **5**, HATU, DIEA, DMF; (e) TFA, DCM; (f) azido-mannose, Cu(I), DMF/H_2O.

Scheme 1: Synthesis and structures of the lipids.

The spectroscopic properties of the glycolipids were studied in acetonitrile, water, and soybean oil (Figure S1). They all display narrow structured absorption and emission bands commonly observed for BODIPY derivatives with small stokes-shifts and little solvatochromism. Clear signs of aggregation are however observable in water for the neutral lipids. The absorption in water of G-mannolipid is broader than expected, while O-mannolipid exhibits an additional red-shifted emission peak centered at 680 nm. The aggregation is less pronounced for the more hydrosoluble charged derivatives. The G-mannolipid (-) presents a narrowed spectrum in water and O-mannolipid (-) shows no additional fluorescence emission peak. This observation is confirmed by the measurement of critical micellar concentration that are one order of magnitude higher (2-3 µM) for the charged derivatives compared to their neutral counterparts (ca. 0.2 µM) (Table S2 and Figure S2). The molar absorptivities and fluorescence quantum yields measured in acetonitrile also confirm that the mannolipids conserve the high brightness of BODIPY fluorophores with the exception of O-mannolipid (-) (Figure 2A). The latter displays a surprisingly low molar absorption coefficient and fluorescent quantum yield compared to its neutral counterpart. The emission and absorption of the green and orange BODIPY overlap well making it an efficient and previously unreported FRET pair

with a Förster radius of 4.6 nm (Figure 2B and Table S3). Thus, we have synthesized a library of lipids having heads and tails easily tunable to functionalize O/W droplets and develop biosensing particles using a FRET pair of lipids.

A

	λ_{abs} (nm)	λ_{em} (nm)	ε ($cm^{-1}.M^{-1}$)	Φ	Brigthness (εφ)
G-mannolipid	498	509	40000	0.50	20000
O-mannolipid	567	582	47000	0.65	31000
G-mannolipid (-)	498	508	40000	0.47	19000
O-mannolipid (-)	567	581	12000	0.39	4680

B

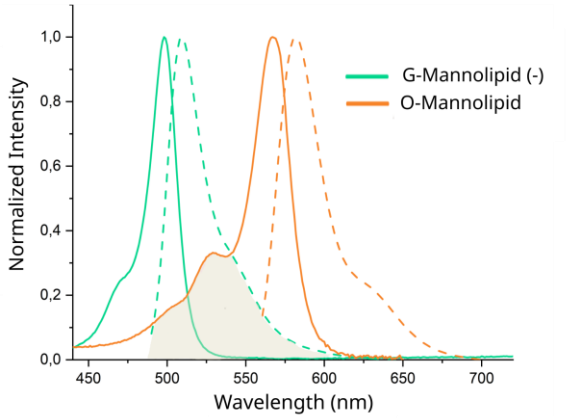

Figure 2: **Spectroscopic properties of lipids. (A)** Spectroscopic data of mannolipids in acetonitrile. λ_{abs}: peak absorption wavelength, ε: molar absorption coefficient, λ_{em}: peak emission wavelength, Φ: fluorescence quantum yield. (B) Spectra of G-mannolipid (-) and O-mannolipid in acetonitrile with absorbance spectra in solid lines and fluorescence spectra in dashed lines. Grey area shows the spectral overlap between donor fluorescence and acceptor absorbance.

Formulation and functionalization of the microparticles. The O/W lipid droplets were formulated with membrane emulsification, lipiodol oil, chosen for its high density allowing easy formulation and Pluronic F68 15% w/w with a 3 µm pore sized membrane, yielding 10 µm droplets with a well-controlled sized (dispersion of 1.7 µm) (Figure S3). These microparticles were functionalized using PB-Tween 20 (at CMC) as surfactant and different concentrations in lipids. Each concentration corresponds to a number of theoretical surface equivalents, with 1 equivalent meaning the theoretical saturation of the surface by the lipids as described by Pinon *et al.*[21] We estimate the surface equivalents by using the previously reported surface occupancy of linear glycolipids (50 Å) and the total surface of the droplet.[14] The precise formulation and functionalization are described in material and methods. The functionalization of the microparticles with different surface equivalents of lipids was

monitored by measuring the fluorescence of the droplets using an epifluorescence microscope after washing the excess of fluorescent glycolipids (Figure 3).

G-mannolipid and G-mannolipid (-) yield classical increasing binding curves that could be fitted to a Langmuir isotherm model with dissociation constants K_D of 0.03 eq and 0.4 eq respectively. (Figure 3A, Figure S4 and Table S4). The introduction of the charge thus enables modulating the formulation of the droplets, with an affinity one order of magnitude lower for the more hydrophilic negatively charged lipid. Interestingly, the fluorescence continues to increase beyond the theoretical surface saturation, showing that the lipids are also able to enter the bulk of the droplets. This is confirmed by the intensity profiles of G-mannolipid-coated droplets plotted at 0.07eq and 4eq of lipid (Figure 3B and Figure 3C). The first profile indicates a surface functionalization while the latter shows a homogeneous localization of the lipid in the droplet. Although there is no visible aggregation-caused quenching, the spectroscopic characterization of the droplets coated with G-mannolipid shows two emission peaks: one at 520 nm and a red-shifted one at 600 nm that typically corresponds to BODIPY J-aggregates.[30,31,32] The addition of the charge in G-mannolipid(-) improves the intensity of fluorescence avoiding the additional J-aggregate emission peak (Figure 3D).

The binding of the O-mannolipid displays a very different trend. After an initial increase of fluorescence, it rapidly decreases, indicating the occurrence of aggregation-caused quenching on the surface of the droplets and, in a third phase, the fluorescence increases again likely due to the penetration of the lipid inside the droplets (Figure 3E, Figure S4 and Table S4). The difference of behavior can be explained by the increased aromatic surface of the O-BODIPY that favors aggregation. Indeed, a high concentration of highly conjugated BODIPYs can lead to self-absorption and strong intermolecular interactions (π-π stacking) induced by their planar structures and small Stokes shift. Most BODIPY thus suffer from aggregation-caused quenching [26,27], which is a well-known phenomenon in loaded particles at high concentration.[33] The early growth phase of the binding curves was fitted to a Langmuir isotherm model as well and yielded Kd values of 0.002 eq and 0.02 eq for O-mannolipid and its charged counterpart respectively. The relative effect of the negative charge on the droplet formulation thus appears to be the same for the G-Mannolipid and O-Mannolipid. The spectral characterization of the O-Mannolipid confirms that adding a negative charge reduces the aggregation-caused quenching as the maximum of fluorescence intensity is increased 2-fold for O-mannolipid (-) (Figure 3F). Interestingly even if the self-quenching is reduced, a novel

emission band appears at 670 nm that could be due to J-aggregates. The behaviors of the G-lactolipid and G-Biotinlipid are very comparable to that of the G-Mannolipid (Figure S4), indicating that the formulation and surface functionalization is mostly governed by the nature of the BODIPY fluorophore, but can be tuned by the addition of a net charge on the polar head.

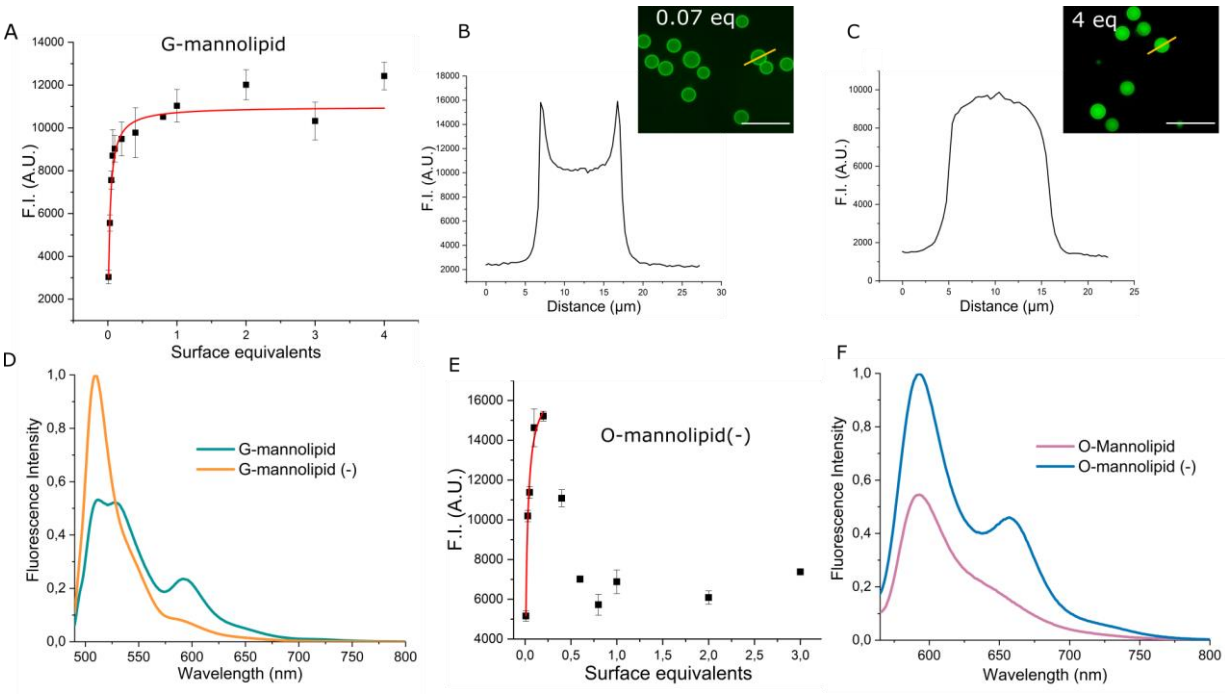

Figure 3: **Functionalization results of G-mannolipid.** (A) Titration of the insertion of G-mannolipid on the surface of the droplets. Error bars represents the standard deviation to the mean intensity measured on 5 wide-field microscopy images for each datapoint. Red line is a fit of the titration curve to a Langmuir adsorption isotherm. (B) Typical intensity profile and corresponding epifluorescence image of unsaturated droplets coated with 0.07 eq in G-mannolipid (GFP excitation and monoband filter). Scale bar 40 µm. (C) Typical intensity profile and corresponding epifluorescence image of saturated droplets coated with 4 eq in G-mannolipid (GFP excitation and monoband filter). (D) Fluorescence spectra of 11 million droplets coated with 0.3 eq of G-mannolipid or G-mannolipid (-). (E) Titration of the insertion of O-mannolipid (-) on the surface of the droplets. Error bars represents the standard deviation to the mean intensity measured on 5 wide-field microscopy images for each datapoint. Red line is a fit of the titration curve to a Langmuir adsorption isotherm. (F) Fluorescence spectra of 11 million droplets coated with 0.3 eq of O-mannolipid or O-mannolipid (-).

Specific recognition of the particles by lectin-receptors in vitro and in primary murine bone-marrow derived macrophages.

We studied the biomimetic properties of our microparticles using lectins receptors. Among the diverse adhesion receptors, lectins represent a huge family of carbohydrate binding

proteins without enzymatic activity present in plants and animals. They identify pathogens associated molecular patterns in a Ca2+ dependent manner. A critical feature is their multivalency allowing interaction with sugars from different glycoproteins, glycolipids on the same cell or different cells thus leading to aggregation of glycoconjugates and aggregation of receptors.[4] For example, mannose terminated oligosaccharides, present on a large panel of unrelated pathogens (viruses[37], fungi[38], bacteria[39]) are targeted by mannose lectins such as Mannose Receptor, DC-sign or dectin during the immunity adhesion processes, and the adhesion of leucocytes to the epithelial surfaces are regulated by L-selectins .[2] Moreover, we also used IgG molecules to demonstrate the versatility of our platform, targeting easily diverse adhesion receptors. IgG molecules are ligands of the cells that cover pathogens to be ingested by immunity cells.[37]

The specific recognition of the mannosylated particles was studied *in vitro* by fluorescence spectroscopy and microscopy using concanavalin A (ConA) as a soluble model of lectins. ConA is a tetravalent lectin that recognizes polysaccharides with terminal mannose pattern but not lactose. Measurements were performed on droplets functionalized with the four mannolipids to study the possible influence of the fluorophore and the charge on the recognition and with the lactolipid as a negative control. First, the spectral properties of the mannosylated droplets were recorded with and without ConA (Figure 4A). Interestingly, upon contact with ConA, the fluorescence intensity of droplets increased for each mannolipid. This may be due to a new arrangement of the fluorophores at the interface of the droplet, reducing the aggregation-caused quenching by destacking of the molecules by the receptor.

In vitro recognition tests were performed by wide-field microscopy using ConA, Peanut agglutinin, (PNA) a control lectin that binds to Gal-β(1-3)-GalNAc and do not recognize mannosides or IgG anti-biotin, all labelled with alexa647 (Deep red channel). Fluorescence intensities of ConA, PNA or IgG anti-biotin were measured after 1h in contact with the droplets coated with G-mannolipid (blue bars), G-lactolipid (grey bar), G-biotin-lipid (purple bar) or naked droplets (green bars) and multiple washing steps to eliminate the excess of unbound receptor. With addition of ConA on G-mannolipid coated droplets, large clusters of mannolipid-coated droplets consistent with the agglutination properties of multivalent lectins were visible as well as a high fluorescence signal on the surface of the droplet in the deep red channel both of which are evidence of the binding of ConA to the mannolipid-coated droplets

(Figure 4B and 4C). This recognition by ConA was observed for all four mannolipids. With addition of ConA on naked droplets, a low deep-red fluorescence of naked droplets indicated non-specific binding was observed meaning that the recognition of the mannolipid-coated droplets was specific (Figure 4C). Interestingly lactolipid-coated droplets in presence of ConA showed an even lower deep-red fluorescence than naked droplets (Figure 4C), indicating that the non-specific binding of naked droplets can be suppressed in the presence of the lactolipid. Thus, it is possible to passivate the droplets and avoid non-specific binding. As an additional negative control, the mannolipid coated droplets were also placed in contact with PNA labeled with alexa 647 that does not recognize mannose. Some signal was detected in the deep-red channel, but it is similar to that observed with naked droplets and thus originates from non-specific binding (Figure 4C and 4D) The specific recognition of the G-biotinlipid by anti-biotin IgG was also evidenced (Figure 4C and 4E). IgG anti-biotin recognizes specifically the droplets coated with the biotin lipid with a deep-red fluorescence increasing with the number of equivalents of lipid. No recognition of naked droplets was observed.

To further evidence the selectivity of the binding, a competitive binding assay was also performed with mannolipid coated droplets in presence of increasing concentration of free mannose (1 mM and 10 mM) or free galactose (10 mM). As expected, when increasing the concentration of mannose, the cluster size decreased as well as the deep red fluorescence signal (Figure 4C and 4F). Conversely, when galactose at the same concentration was added the fluorescence intensity was not changing. The recognition by Con A is thus specific to the mannolipid at the surface of the droplet.

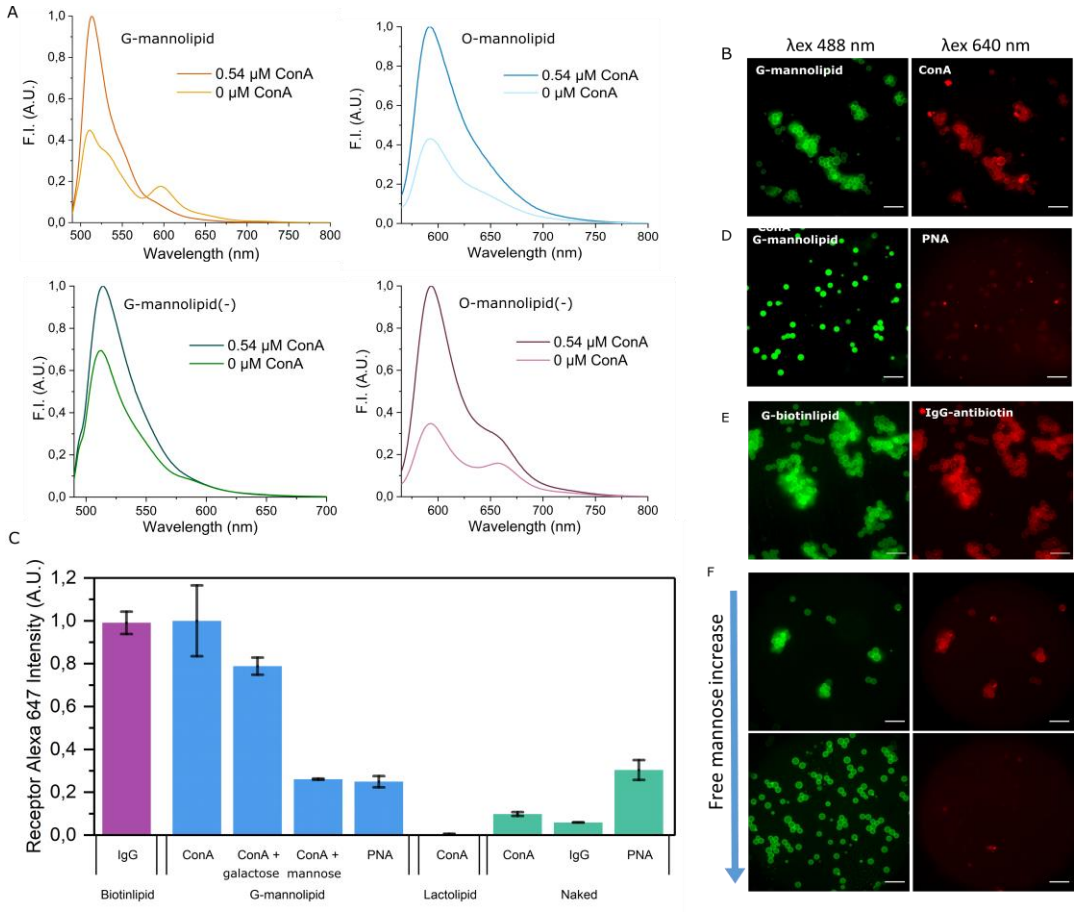

Figure 4**: Specific recognition tests in vitro.** (A) Fluorescence spectra of 5.5 million droplets coated with 0.3 eq of mannolipids in presence or in absence of ConA. (B) Epi-fluorescence images of droplets coated with 2 eq of G-mannolipid in presence of 0.48 µM ConA alexa 647. (C) Fluorescence intensity of ConA (0.48 µM), peanut agglutinin (0.48 µM) or IgG-anti-biotin alexa (0.23 µM) labeled with Alexa 647 measured upon contact with droplets either coated with 2 eq of various lipids (see legend) or naked. Error bars represents the standard deviation to the mean intensity measured on 5 wide-field microscopy images for each datapoint. (D) Epi-fluorescence images of droplets coated with 2 eq of G-mannolipid coated in presence of 0.48 µM PNA alexa 647. (E) Epi-fluorescence images of droplets coated with 2 eq of G-biotinlipid coated in presence of IgG anti-biotin alexa 647. (F) Epi-fluorescence images of 2 eq G-mannolipid coated particles in presence of 0.48 µM ConA alexa 647 and competing mannose (top: 1 mM mannose, bottom: 10 mM mannose).

As a model of adhesion processes, we have selected phagocytosis, a mechanism of internalization of micrometer-sized particulate material and performed by macrophages as part of the immune response. As all cell adhesion phenomenon, it is triggered by the recognition of ligands of pathogens such as sugars patterns by an array of receptors present at the surface of the cell that promotes adhesion of the membrane to the pathogen.[4] To investigate the recognition of the mannolipid-coated particles by specific adhesion receptors, we analyzed the interaction of mannolipid-coated droplets with primary murine macrophages

derived from bone-marrow precursors obtained as described by Marion *et al*. [34] The macrophages were incubated at 37°C with naked (green bars) or mannolipid-functionalized (blue and gray bars) lipid droplets (Figure 5A and 5B). When indicated, the cells were pretreated with soluble mannan. for 20 min prior to incubation with the functionalized droplets. After 10 min of contact, the association index, *i.e.* the mean number of droplets associated (internal or external) with the cells, was calculated. Macrophages incubated with naked droplets or pretreated with soluble mannan exhibited a significantly lower binding and phagocytic activity, as compared with untreated macrophages incubated with mannolipid-coated droplets. These results demonstrate a specific binding and phagocytosis of the mannolipid-coated particles in primary murine professional phagocytic cells.

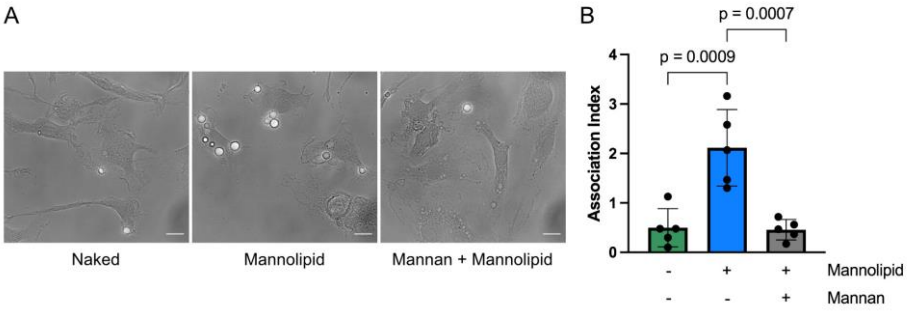

Figure 5: **Specific recognition and phagocytosis tests with primary murine bone-marrow derived macrophages.** Primary murine bone-marrow derived macrophages were treated for 20 min with soluble mannan (10 mg/mL, grey bar) or not (green and blue bars) prior to be incubated with naked droplets (green bars) or G-mannolipid-coated droplets (0.5 eq, blue and grey bars) for 10 min at 37°C. (A) Brightfield images of cells with associated droplets. One representative field for each condition is shown. Scale bar = 10 μm. (B) Average number of associated particles per cell was calculated in 25-30 cells per condition. The means ± SD of 5 independent experiments are plotted.

FRET to study the binding with lectin receptors. To evidence the possibility of monitoring receptor binding via FRET, the tunable microparticles were functionalized with G-mannolipid (-) and O-mannolipid. The two lipids were chosen since their spectral properties are simpler, with no additional aggregate emission peaks that could complexify FRET measurements. The 4 binding sites of ConA are approximately separated by 5 nm which corresponds to the Förster radius of our FRET pair (Table S3 and Figure S5). If the two mannolipids bind to different sites of ConA, the distance between them should be ideal to observe a FRET signal.

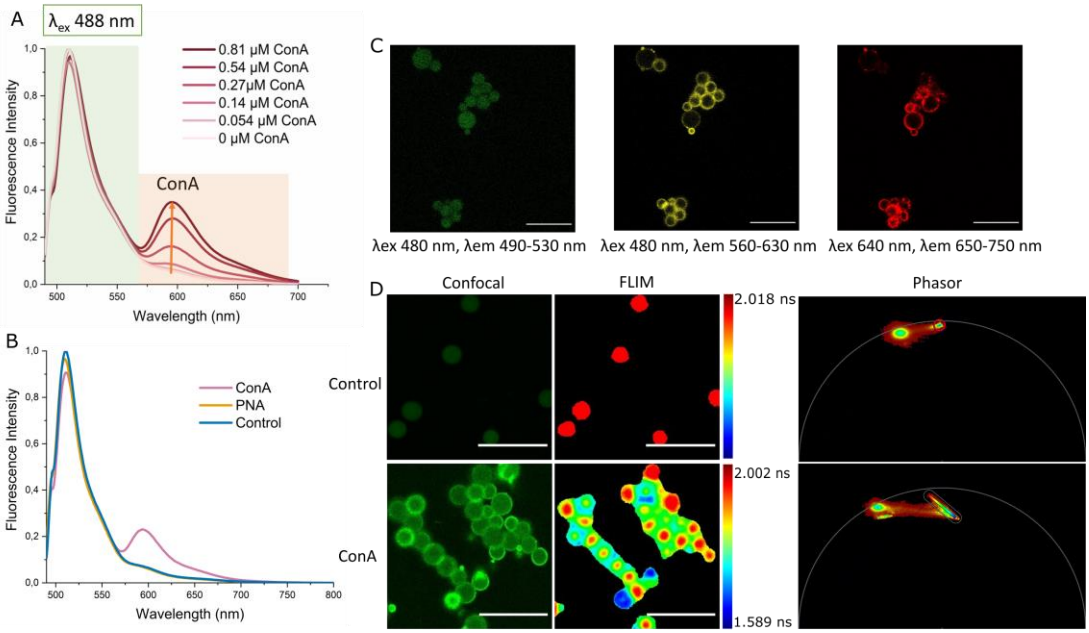

Figure 6: **FRET experiments.** (A) Typical fluorescence spectra of 5.5 million droplets simultaneously coated with 0.3 eq G-mannolipid (-) and 0.3 eq O-mannolipid in presence of different concentrations of ConA when exciting at 488 nm. (B) Fluorescence spectra of 3.6 million droplets simultaneously coated with 0.3 eq G-mannolipid (-) and 0.3 eq O-mannolipid in presence of either ConA (0.54 µM) or PNA (0.51 µM). (C) Confocal images of 5.5 million droplets simultaneously coated with 0.3 eq G-mannolipid (-) and 0.3 eq O-mannolipid in presence of 0.27 µM ConA alexa 647. (D) Typical confocal and FLIM images with phasor representation of 5.5 million droplets simultaneously coated with 0.3 eq G-mannolipid (-) and 0.3 eq O-mannolipid in presence or not of 0.54 µM ConA. The fluorescence intensity and lifetimes measured are those of the donor: λ_{exc} = 488 nm, collection: 498 nm – 530 nm.

Droplets were functionalized with 0.3 eq G-mannolipid (-) and 0.3 eq O-mannolipid. This concentration was chosen so as to not saturate the surface and keep the mobility of the lipids while still allowing efficient recognition by the receptors. Different concentrations of ConA were added to control the changes in fluorescence emission with the receptor concentration. The spectroscopic results are presented Figure 6A and S8. As discussed above, the emission of the donor increases upon binding of the droplets to ConA. Due to this competing phenomenon, FRET cannot be measured by monitoring the decrease of the fluorescence of the donor. The energy transfer is however clearly visible by recording the fluorescence emission of the acceptor. The emission band of O-mannolipid (λ_{em} 600 nm) increased with the concentration of ConA when exciting the donor at 480 nm, revealing the FRET phenomenon. A control experiment verified that excitation of the droplets functionalized with the acceptor

O-mannolipid alone at 480 nm leads to only a residual fluorescence signal with or without ConA (Figure S6 and S7).

To confirm that FRET is indeed linked to the binding to ConA, a control test was performed with Peanut agglutinin and the acceptor emission arising from energy transfer was only visible in the presence of ConA (Figure 6B).

FRET was also studied by steady-state and time-resolved confocal microscopy. Firstly, the droplets functionalized with G-mannolipid (-) and O-mannolipid were observed in presence of ConA alexa 647. The emission of G-mannolipid (-) was observed in the green channel (λ_{ex} 480 nm, λ_{em} 490-530 nm), the FRET-sensitized O-mannolipid fluorescence in the yellow channel (λ_{ex} 480 nm, λ_{em} 560-630 nm) and the ConA alexa 647 in the red channel (λ_{ex} 640 nm, λ_{em} 650-750 nm). The fluorescence of the donor was visible in the whole droplet, while the FRET signal was located only at the surface of the droplet as was the labelled ConA (Figure 6C). This shows that FRET is indeed concomitant to the binding of ConA to the mannolipids. The droplets co-functionalized with G-mannolipid (-) and O-mannolipid were then studied with two different concentrations of unlabeled conA (Figure S7). Direct excitation of either the donor of the acceptor showed fluorescence in the whole droplets, but the FRET-sensitized emission of the acceptor, was only visible on the surface of the droplets and increased with the concentration of receptor. FRET between two lipids thus enables the specific detection of the binding of the unlabeled cognate receptor at the surface of the droplet.

Since FRET cannot be monitored via the emission of the donor, no quantitative FRET measurement is possible by steady-state fluorescence, and we have thus performed time-resolved FRET by FLIM microscopy. Droplets were functionalized with 0.3 eq G-mannolipid (-) and 0.3 eq O-mannolipid. The lifetime of G-mannolipid (-) was measured using FLIM before and after adding ConA (Figure 6D). Without ConA, the phasor plot of the donor shows only a single population with a nearly monoexponential lifetime. Upon addition of ConA, a decrease of the donor fluorescence lifetime is visible (Figure 6D and Table S5), thus evidencing the FRET in our microparticles due to the recognition with ConA. The FRET efficiency E was calculated to be 21±1% with Δt=0.41±0.04 ns. Colocalization analysis in fluorescence microscopy, while popular for indicating potential associations between molecules based on overlapping fluorescence signals, doesn't directly prove molecular recognition. Microscopes resolution limits (~200-300 nm) mean that colocalized signals might just be close, not necessarily interacting. On the contrary, this FRET-sensing tool allows visualizing short-range interaction

well below this resolution limit (at a 10 nm distance) and to unambiguously detect the binding of ConA to the mannolipids at the surface of the particle.

3. CONCLUSION

We have created an adaptable platform using lipids-coated fluorescent microparticles to sense adhesion phenomena. We have synthesized and characterized a series of fluorescent lipids with various targeting heads and fluorescent tails. These biomimetic particles interact with receptors in vitro, forming clusters. They are bound and phagocytosed in a receptor specific manner by primary macrophages. A novel BODIPY FRET pair was developed, allowing in vitro FRET between glycolipids localized at the surface of microparticles to study receptor binding. Our results confirm the biosensing platform's utility in revealing short-range interactions, thus providing clear evidence of specific receptor recognition. We have developed a unique tool to evidence and visualize receptor binding that could help study on adhesion mechanism. The design is modular and can be easily adapted to obtain different fluorescence emissions and to target diverse receptors. Adhesion processes usually involve different receptors, and we can envision in the future that FRET could also be used to detect the binding of two different cooperating receptors. In particular, these glycosylated particles could be used to study the role of lectins in phagocytosis.

4. EXPERIMENTAL METHODS

Synthesis

Synthesis and characterization of lipids are described in the Supporting Information.

Droplets formulation

A Shirasu porous glass (SPG) apparatus with a membrane having a 3µm pore size was used. The membrane was immersed into an aqueous phase of Pluronic F68 block-copolymer surfactant at 15 wt %. The dispersed phase (oil) was inserted in a reservoir connected by a pressure valve. Then, pressure was applied to the dispersed phase that finally crossed the membrane after reaching the critical pressure of the membrane. A concentrated emulsion of droplets with a defined size of 10.0 µm ± 1.7 is obtained.

Droplets functionalization

References of products are described in the Supporting Information.

The functionalization of droplets and recognition by ConA for sugar lipids was performed following this procedure:

10µL of 10 µm droplets i.e. 11 million droplets in Pluronic F68 15 wt % were placed in a microtube and the tube was completed to 200 µL with PB Tween 20 CMC. The diluted emulsion was centrifuged at 2000 rpm for 30 sec. 190 µL were removed and 190 µL of PB-Tween were added again. This washing-step was repeated 3 times. Then, a volume of the probe correspondent to the number of equivalents desired (for 1 eq: 12µL) was added to the solution followed by DMSO as polar solvent (total volume of addition 20 µL so for 1 equivalent: 8 µL of DMSO). After an hour rotation, washing steps were repeated three times this time with PBS containing $CaCl_2$ 0.1 mM and $MnCl_2$ 0.1 mM for mannolipids and lactolipid, and with PB-Tween 20 CMC for biotinlipid. 30 µL were observed on a glass slide within a chamber.

Epifluorescence microscopy was performed on a Zeiss Axioimager Z1 equipped with a lumencor spectraX light source with GFP monoband filter for green lipids, Cy3 monoband filter for orange lipids and deep red multiband filter for proteins labeled with Alexa 647.

Droplets recognition in vitro and with Primary murine bone-marrow derived macrophages

References of products can be found in the Supporting Information.

For in vitro tests recognition with mannolipids and lactolipid, 10 µL (1 mg/mL initial concentration in sodium bicarbonate) ConA stained with Alexa Fluor 647 or Peanut agglutinin with Alexa Fluor 647 were added to 11 million 10 µm droplets functionalized droplets meaning 0.48 µM final concentration. The solution was rotated 1 hour then washed with the solution of PBS three times again. For the test with free mannose and galactose, solutions of sugars were prepared at 100 mM in water and added at the same time than ConA. For biotin lipid the same procedure was used with 9µL of IgG-anti-biotin Alexa 647 at 0.85 mg/mL meaning 0.23 µM final concentration. 30 µL were observed on a glass slide within a chamber with epi-fluorescence microscopy, Deep red filter for receptors.

Binding and phagocytic assay were performed in primary murine bone-marrow derived macrophages cultivated from 6–8-week-old mice femoral and tibial bones. Briefly, the cell suspensions were depleted in red blood cells for 2 min at room temperature in NH4Cl red blood cell lysis buffer, then plated with 20 ng/mL of mouse M-CSF in complete medium

consisting of RPMI Glutamax supplemented with 10 % Fetal Calf serum, 10 mM HEPES, 1 mM sodium pyruvate, 50 mM beta-mercaptoethanol (all from Gibco) in Petri dishes for 8 days at 37°C with 5% CO2. The cells were then washed and resuspended in PBS1X before being diluted at 1/3 and plated in complete medium for 3 more days. Macrophages were then washed in PBS1X, resuspended and pelleted before being plated in complete medium in a Falcon culture dish containing glass coverslips overnight at 37°C. 4 μm size lipid droplets were prepared using a 1.1 μm pore size membrane and functionalized as described above with 0.5 eq G-mannolipid. 30 particles per cell (6X10^6 droplets/coverslip) were used for experiments. When indicated, the macrophages were treated with 10 mg/mL of soluble mannan for 20 min at 37°C prior to incubation with the droplets. After 10 min at 37°C, the cells were fixed with 4% paraformaldehyde for 45 min at 4°C, then washed and incubated for 10 min with 50 mM NH4Cl in PBS1X, and then washed in PBS1X. The cells were then permeabilized in 2% FCS 0.05% saponin in PBS1X and incubated in the same buffer containing Phalloidin Alexa546 for 25 min at room temperature. After three washes in the permeabilization buffer and one wash in PBS1X, the cells were incubated with DAPI (DiAmidino Phenyl Indole) at 1/30 000 in PBS1X and then mounted on microscopy slides with 5 μl of Fluoromount G. External and internalized particles were counted in 25-30 randomly chosen cells, and the mean number of cell-associated (bound + internalized) particle was calculated. Images were acquired using an inverted wide-field microscope (Leica DMI6000) with a 100× (1.4 NA) objective and a (MicroMAX Princeton Instruments) camera. Statistical significance was determined by One-Way ANOVA test (Prism software version 9.5.0).

Spectroscopic characterization

Additional spectroscopic characterizations are described in the Supplementary Information.

For the analysis of droplets coated with one single lipid by fluorescence spectroscopy, 100 μL of solution containing 5.5 million (10 μm) droplets functionalized at 0.3 eq of each lipid were added to 600 μL of PBS and mixed before measuring. For the analysis of droplet coated with two lipids by fluorescence spectroscopy, 100 μL of solution containing 5 million droplets functionalized at 0.3 eq of each lipid were added to 600 μL of PBS. When necessary, unstained ConA (2 mg/ mL initial concentration in sodium bicarbonate) or unstained peanut agglutinin (1 mg/mL in water) were added to the solution and mixed.

Droplets imaging

Confocal images were recorded on a Leica SP8 with a 63X oil immersion objective. 30 µL of 5.5 million 10 µm droplets functionalized with 0.3 eq G-mannolipid (-) and 0.3 eq O-mannolipid (V= 3.6 µL of 1 mM solution in DMSO) were imaged in a glass slide chamber. ConA unstained at 2 mg/ml initial concentration was used when needed with the same procedure as for the droplets recognition tests. For G-mannolipid (-): ex 488, 499-530, for O-mannolipid FRET emission: ex 488, 560-648, for O-mannolipid: ex 550, 560-648, for ConA emission: ex 640, 650-750. FLIM measurements were recorded on a SR Leica SP8X FLIM with a 63X oil immersion objective. FLIM phasor plot representation was obtained using a pulse laser, a median filter and a hybrid count detector with excitation at 488 nm, emission 498-530 nm. FLIM measurements were performed on 3 independent experiments of functionalized droplets with 0.3 eq G-mannolipid (-) and O-mannolipid. For FRET measurements 0.54 µM ConA was added during 1 hour before imaging.

The FRET efficiency *E* was calculated using the lifetime of the donor in presence of acceptor without receptor τ_A and the minimum lifetime achieved of the donor in presence of acceptor and receptor τ_B :

$$E = 1 - \frac{\tau_B}{\tau_A}$$

Error bars represents the standard deviation to the mean FRET efficiency measured on 4 confocal microscopy images on three independent experiments.

ASSOCIATED CONTENTS

Supporting Information:

- Material and methods
- Spectroscopic additional results
- Functionalization additional results
- FRET in droplets analysis complements
- Synthetic methods

AUTHOR INFORMATION

Notes: the authors declare no conflict of interest

Corresponding authors

***blaise.dumat@ens.psl.eu**

***Jean-maurice.mallet@ens.psl.eu**

Authors contribution

Sophie Michelis: Conceptualization, Methodology, Validation, Formal analysis, Investigation, Writing-original draft, Visualization. Chiara Pompili: Conceptualization, Investigation, Methodology, Validation, Formal analysis, Visualization. Florence Niedergang: Conceptualization, Supervision, Writing-Review&Editing, Funding acquisition. Jacques Fattaccioli: Conceptualization, Supervision, Writing-Review&Editing, Funding acquisition. Blaise Dumat: Conceptualization, Methodology, Validation, Writing-Review&Editing, Supervision. Jean-Maurice Mallet: Conceptualization, Methodology, Supervision, Writing-Review&Editing, Funding acquisition.

ACKNOWLEDGMENTS

This work is supported by a collaborative grant between FN, JMM and JF (ANR-20-CE13-0017-01). Work in the laboratory of FN was also supported by grants from CNRS, INSERM, Université Paris Cité. CP is a student from the FIRE PhD program funded by the Bettencourt Schueller foundation and the EURIP graduate program (ANR-17-EURE-0012). CP is supported by PhD fellowship CNRS 80 Prime and ANR. CP and FN thank Floriane Herit for her help in generating the bone-marrow-derived macrophages. We thank the IMAG'IC facility of Institut Cochin that is part of the national France-BioImaging infrastructure supported by the French National Research Agency (ANR-10-INBS-04).

REFERENCES

(1) Ahmad Khalili, A.; Ahmad, M. R. A Review of Cell Adhesion Studies for Biomedical and Biological Applications. *Int J Mol Sci* **2015**, *16* (8), 18149–18184. https://doi.org/10.3390/ijms160818149.
(2) Ivetic, A.; Hoskins Green, H. L.; Hart, S. J. L-Selectin: A Major Regulator of Leukocyte Adhesion, Migration and Signaling. *Frontiers in Immunology* **2019**, *10*.
(3) Changede, R.; Sheetz, M. Integrin and Cadherin Clusters: A Robust Way to Organize Adhesions for Cell Mechanics. *BioEssays* **2017**, *39* (1), e201600123. https://doi.org/10.1002/bies.201600123.
(4) Depierre, M.; Jacquelin, L.; Niedergang, F. *Phagocytosis*, Gerald. W. Hart, Ralph A. Bradshaw, and Philip D Stahl, editor.; In Encyclopedia of Cell Biology, 2nd edition; Elsevier, 2022; Vol. 3, 286–295.

(5) Cummings, R. D. “Stuck on Sugars – How Carbohydrates Regulate Cell Adhesion, Recognition, and Signaling.” *Glycoconj J* **2019**, *36* (4), 241–257. https://doi.org/10.1007/s10719-019-09876-0.
(6) Baranov, M. V.; Kumar, M.; Sacanna, S.; Thutupalli, S.; van den Bogaart, G. Modulation of Immune Responses by Particle Size and Shape. *Front Immunol* **2020**, *11*, 607945. https://doi.org/10.3389/fimmu.2020.607945.
(7) Champion, J. A.; Mitragotri, S. Shape Induced Inhibition of Phagocytosis of Polymer Particles. *Pharm Res* **2009**, *26* (1), 244–249. https://doi.org/10.1007/s11095-008-9626-z.
(8) Hirota, K.; Hasegawa, T.; Hinata, H.; Ito, F.; Inagawa, H.; Kochi, C.; Soma, G.-I.; Makino, K.; Terada, H. Optimum Conditions for Efficient Phagocytosis of Rifampicin-Loaded PLGA Microspheres by Alveolar Macrophages. *Journal of Controlled Release* **2007**, *119* (1), 69–76. https://doi.org/10.1016/j.jconrel.2007.01.013.
(9) Hao, N.; Neranon, K.; Ramström, O.; Yan, M. Glyconanomaterials for Biosensing Applications. *Biosens Bioelectron* **2016**, *76*, 113–130. https://doi.org/10.1016/j.bios.2015.07.031.
(10) Gupta, A.; Gupta, G. S. Applications of Mannose-Binding Lectins and Mannan Glycoconjugates in Nanomedicine. *J Nanopart Res* **2022**, *24* (11), 228. https://doi.org/10.1007/s11051-022-05594-1.
(11) Wijagkanalan, W.; Kawakami, S.; Takenaga, M.; Igarashi, R.; Yamashita, F.; Hashida, M. Efficient Targeting to Alveolar Macrophages by Intratracheal Administration of Mannosylated Liposomes in Rats. *Journal of Controlled Release* **2008**, *125* (2), 121–130. https://doi.org/10.1016/j.jconrel.2007.10.011.
(12) Yeeprae, W.; Kawakami, S.; Yamashita, F.; Hashida, M. Effect of Mannose Density on Mannose Receptor-Mediated Cellular Uptake of Mannosylated O/W Emulsions by Macrophages. *Journal of Controlled Release* **2006**, *114* (2), 193–201. https://doi.org/10.1016/j.jconrel.2006.04.010.
(13) Argudo, P. G.; Spitzer, L.; Ibarboure, E.; Jerome, F.; Cramail, H.; Lecommandoux, S. Mannose-Based Surfactant as Biofunctional Nanoemulsion Stabilizer. *Colloids and Surfaces B: Biointerfaces* **2022**, *220*, 112877. https://doi.org/10.1016/j.colsurfb.2022.112877.
(14) Dumat, B.; Montel, L.; Pinon, L.; Matton, P.; Cattiaux, L.; Fattaccioli, J.; Mallet, J.-M. Mannose-Coated Fluorescent Lipid Microparticles for Specific Cellular Targeting and Internalization via Glycoreceptor-Induced Phagocytosis. *ACS Appl. Bio Mater.* **2019**, *2* (11), 5118–5126. https://doi.org/10.1021/acsabm.9b00793.
(15) Yang, G.; Liu, Y.; Teng, J.; Zhao, C.-X. FRET Ratiometric Nanoprobes for Nanoparticle Monitoring. *Biosensors* **2021**, *11* (12), 505. https://doi.org/10.3390/bios11120505.
(16) Bou, S.; Klymchenko, A. S.; Collot, M. Fluorescently Labeled Branched Copolymer Nanoparticles for *In Situ* Characterization of Nanovectors and Imaging of Cargo Release. *ACS Appl. Nano Mater.* **2022**, *5* (3), 4241–4251. https://doi.org/10.1021/acsanm.1c04582.
(17) Tretiakova, D. S.; Alekseeva, A. S.; Galimzyanov, T. R.; Boldyrev, A. M.; Chernyadyev, A. Yu.; Ermakov, Yu. A.; Batishchev, O. V.; Vodovozova, E. L.; Boldyrev, I. A. Lateral Stress Profile and Fluorescent Lipid Probes. FRET Pair of Probes That Introduces Minimal Distortions into Lipid Packing. *Biochimica et Biophysica Acta (BBA) - Biomembranes* **2018**, *1860* (11), 2337–2347. https://doi.org/10.1016/j.bbamem.2018.05.020.
(18) Klymchenko, A. S.; Roger, E.; Anton, N.; Anton, H.; Shulov, I.; Vermot, J.; Mely, Y.; Vandamme, T. F. Highly Lipophilic Fluorescent Dyes in Nano-Emulsions: Towards Bright Non-Leaking Nano-Droplets. *RSC Adv.* **2012**, *2* (31), 11876–11886. https://doi.org/10.1039/C2RA21544F.
(19) Pan, Y.; Nitin, N. Real-Time Measurements to Characterize Dynamics of Emulsion Interface during Simulated Intestinal Digestion. *Colloids and Surfaces B: Biointerfaces* **2016**, *141*, 233–241. https://doi.org/10.1016/j.colsurfb.2016.01.053.
(20) Zhang, J.; Lv, Y.; Wang, B.; Zhao, S.; Tan, M.; Lv, G.; Ma, X. Influence of Microemulsion–Mucin Interaction on the Fate of Microemulsions Diffusing through Pig Gastric Mucin Solutions. *Mol. Pharmaceutics* **2015**, *12* (3), 695–705. https://doi.org/10.1021/mp500475y.

(21) Pinon, L.; Montel, L.; Mesdjian, O.; Bernard, M.; Michel, A.; Ménager, C.; Fattaccioli, J. Kinetically Enhanced Fabrication of Homogeneous Biomimetic and Functional Emulsion Droplets. *Langmuir* **2018**, *34* (50), 15319–15326. https://doi.org/10.1021/acs.langmuir.8b02721.
(22) Merrill, A. H.; Vu, M. N. Glycolipids. In *Encyclopedia of Cell Biology*; Bradshaw, R. A., Stahl, P. D., Eds.; Academic Press: Waltham, 2016; pp 180–193. https://doi.org/10.1016/B978-0-12-394447-4.10022-7.
(23) Loudet, A.; Burgess, K. BODIPY Dyes and Their Derivatives: Syntheses and Spectroscopic Properties. *Chem. Rev.* **2007**, *107* (11), 4891–4932. https://doi.org/10.1021/cr078381n.
(24) M. Ravikanth, M.; Vellanki, L.; Sharma, R. Functionalized Boron-Dipyrromethenes and Their Applications. *ROC* **2016**, 1. https://doi.org/10.2147/ROC.S60504.
(25) Ni, Y.; Zeng, L.; Kang, N.-Y.; Huang, K.-W.; Wang, L.; Zeng, Z.; Chang, Y.-T.; Wu, J. Meso-Ester and Carboxylic Acid Substituted BODIPYs with Far-Red and Near-Infrared Emission for Bioimaging Applications. *Chemistry – A European Journal* **2014**, *20* (8), 2301–2310. https://doi.org/10.1002/chem.201303868.
(26) Liu, Z.; Jiang, Z.; Yan, M.; Wang, X. Recent Progress of BODIPY Dyes With Aggregation-Induced Emission. *Front. Chem.* **2019**, *7*, 712. https://doi.org/10.3389/fchem.2019.00712.
(27) Marfin, Y. S.; Banakova, E. A.; Merkushev, D. A.; Usoltsev, S. D.; Churakov, A. V. Effects of Concentration on Aggregation of BODIPY-Based Fluorescent Dyes Solution. *J Fluoresc* **2020**, *30* (6), 1611–1621. https://doi.org/10.1007/s10895-020-02622-y.
(28) Descalzo, A. B.; Ashokkumar, P.; Shen, Z.; Rurack, K. On the Aggregation Behaviour and Spectroscopic Properties of Alkylated and Annelated Boron-Dipyrromethene (BODIPY) Dyes in Aqueous Solution. *ChemPhotoChem* **2020**, *4* (2), 120–131. https://doi.org/10.1002/cptc.201900235.
(29) Reisch, A.; Klymchenko, A. S. Fluorescent Polymer Nanoparticles Based on Dyes: Seeking Brighter Tools for Bioimaging. *Small* **2016**, *12* (15), 1968–1992. https://doi.org/10.1002/smll.201503396.
(30) Kim, S.; Bouffard, J.; Kim, Y. Tailoring the Solid-State Fluorescence Emission of BODIPY Dyes by Meso Substitution. *Chemistry – A European Journal* **2015**, *21* (48), 17459–17465. https://doi.org/10.1002/chem.201503040.
(31) Vu, T. T.; Dvorko, M.; Schmidt, E. Y.; Audibert, J.-F.; Retailleau, P.; Trofimov, B. A.; Pansu, R. B.; Clavier, G.; Méallet-Renault, R. *Understanding the Spectroscopic Properties and Aggregation Process of a New Emitting Boron Dipyrromethene (BODIPY)*. ACS Publications. https://doi.org/10.1021/jp3097555.
(32) Tian, D.; Qi, F.; Ma, H.; Wang, X.; Pan, Y.; Chen, R.; Shen, Z.; Liu, Z.; Huang, L.; Huang, W. Domino-like Multi-Emissions across Red and near Infrared from Solid-State 2-/2,6-Aryl Substituted BODIPY Dyes. *Nat Commun* **2018**, *9* (1), 2688. https://doi.org/10.1038/s41467-018-05040-8.
(33) Andreiuk, B.; Reisch, A.; Bernhardt, E.; Klymchenko, A. S. Fighting Aggregation-Caused Quenching and Leakage of Dyes in Fluorescent Polymer Nanoparticles: Universal Role of Counterion. *Chemistry – An Asian Journal* **2019**, *14* (6), 836–846. https://doi.org/10.1002/asia.201801592.
(34) Marion, S.; Mazzolini, J.; Herit, F.; Bourdoncle, P.; Kambou-Pene, N.; Hailfinger, S.; Sachse, M.; Ruland, J.; Benmerah, A.; Echard, A.; Thome, M.; Niedergang, F. The NF-KB Signaling Protein Bcl10 Regulates Actin Dynamics by Controlling AP1 and OCRL-Bearing Vesicles. *Developmental Cell* **2012**, *23* (5), 954–967. https://doi.org/10.1016/j.devcel.2012.09.021.